Journal of the European Ceramic Society **11** (1993) 69–75

Influence of Heterovalent Doping on the Degradation Properties of Lead Magnesium Niobate

O. Noblanc, C. Deljurie & P. Gaucher

Thomson-CSF, Laboratoire Central de Recherches, Groupe Chimie et Céramiques, Domaine de Corbeville, 91404 Orsay Cedex, France

(Received 4 October 1991; revised version received 20 March 1992; accepted 25 March 1992)

Abstract

The perovskite material ABO_3 with A = Pb and B = (Mg, Nb, Ti) has been doped with donors and acceptors in sites A and B. Because of the peculiar properties of this material (ordered nanodomains within a disordered phase), the effects of the dopants are different from those observed for classical perovskites like $BaTiO_3$. Mn and W improve the degradation properties during the accelerated life test. This is interpreted by the built-in internal field observed after the degradation test on the ferroelectric hysteresis loops. This internal field is due to dipolar associated defects also responsible for ageing.

Perovskitmaterialien der Zusammensetzung ABO_3, A = Pb und B = (Mg, Nb, Ti) wurden mit Donoren und Akzeptoren auf Gitterplätzen vom Typ A und B dotiert. Aufgrund der speziellen Struktureigenschaften dieser Materialien (geordnete Nanodomäne eingebettet in eine ungeordnete Matrix), zeigt die Dotierung andere Effekte als in klassischen Perovskitmaterialien wie $BaTiO_3$. Die Autoren finden eine Verbesserung der Alterungseigenschaften unter Dotierung mit Mn und W. Dies wird durch den Einguß eines inneren Feldes zurückgeführt, das durch assoziierte Defekte mit Dipolmoment erzeugt wird. Der Nachweis des inneren Feldes erfolgt in Hysteresemessungen, die nach dem Alterungstest durchgeführt wurden.

Le matériau pérovskite ABO_3 avec A = Pb et B = (Mg, Nb, Ti) a été dopé avec des donneurs et des accepteurs en site A et B. En raison des propriétés particulières de ce matériau (présence de nanodomaines ordonnés dans une matrice désordonnée), l'effet des dopants est différent de celui observé sur les pérovskites plus classiques comme $BaTiO_3$. Mn et W améliorent l'endurance durant le test de dégradation accélérée. Cela est interprété par la présence d'un champ interne observé sur les cycles d'hystérésis après le test de dégradation. Ce champ interne est dû à des défauts associés ayant un moment dipolaire et également responsables du vieillissement en l'absence de champ extérieur.

1 Introduction

Lead magnesium niobate (PMN) is the basic material for new dielectric formulations leading to the Z5U capacitor. Because of its particular ferroelectric properties, very high dielectric constant near the apparent Curie point (due to a relaxation behaviour of the ferroelectric phase) and slim hysteresis loop, it belongs to the family of 'relaxor ferroelectrics'. By shifting the Curie point up to 25°C with $PbTiO_3$ (PT) addition, one can obtain a dielectric constant larger than 22 000 with low dielectric loss tangent (less than 0·03) and the temperature stability of the Z5U standard.

The defect chemistry of this material is not yet well understood because of the heterogeneous nature of the crystal, even in the paraelectric phase. The whole material can be described by the chemical formula

$$\mathrm{PMN} = x[\mathrm{Pb}^{2+}(\mathrm{Mg}^{\mathrm{II}}_{1/2}\mathrm{Nb}^{\mathrm{V}}_{1/2})^{+7/2}\mathrm{O}_3] + (1-x)[\mathrm{Pb}^{2+}(\mathrm{Mg}_{1/3}\mathrm{Nb}_{2/3+x/10})\mathrm{O}_3]$$

where the first term within square brackets represents nanodomains with the Mg and Nb ions ordered on the B site of the perovskite, and the second term represents the disordered matrix in

Journal of the European Ceramic Society 0955-2219/93/$6.00

which the nanodomains are randomly dispersed. As shown in this formula, the ordered domains are electrically charged and behave like acceptors[1] compensated by an excess of niobium. This excess can be approximated by $x/10$ (if the molar content of the ordered phase x is assumed to be much smaller than unity), and the exact value would be given by

$$y = x/10(1-x)$$

The size of the ordered domains results from a compromise between the increase of potential energy due to their electrostatic charge and the decrease of potential energy due to their lower elastic stress (the disordered phase is stressed because of the great difference in size between the Mg and Nb cations).[2]

The nature of the paraelectric–ferroelectric transition is also not yet understood, but the ferroelectric nature of the low-temperature phase is undoubted, because of the presence of a strong and reversible remanent polarization below -30°C, and also because the lattice strain is visible by extended X-ray or neutron diffraction studies.[3] At these low temperatures where most of the material has become ferroelectric, the polar domains are supposed to spread within the disordered phase, in spite of the possibility that their nucleation has been favoured by the ordered domains. According to these previously cited results, it can be assumed that at temperatures lower than -30°C PMN is likely to be a conventional ferroelectric with properties similar to lead zirconate–titanate (PZT) or barium titanate (BT) at room temperature.

In this paper the authors have not investigated the wide and conflicting temperature region lying between -30 and $+150$°C, where the diffuse phase transition occurs. Instead, the authors will try to relate the degradation phenomena occurring in the paraelectric phase at more than 200°C to the ferroelectric properties of the resulting material after cooling down to the true ferroelectric phase. To relate the degradation to defect chemistry, the material was doped with dopants able to modify the concentration of oxygen vacancies—that is, heterovalent dopants of donor, acceptor and mixed valency type in site A or B.

2 Ceramic Processing

PMN–PT powder with 5% PT was prepared by the columbite method developed by Shrout & Halliyal.[4] An excess of magnesium has been used in the $MgNb_2O_6$ in order to neutralize the unreacted niobium responsible for the formation of pyrochlore phase. As a consequence of the very small amount of pyrochlore, no lead excess was necessary for improving the sintering properties. After sintering at 950°C for 4 h in a lead atmosphere, the grain size of the ceramic was about 4 microns, providing a dielectric constant of 22 000 for the non-doped composition. 'A-Site' dopants (donor La, acceptor Na and mixed valency Ag) are introduced by substitution of lead instead of 'B-site' dopants, which are in addition to Mg, Nb and Ti ions, according to the formula

$$Pb_{1-x}A_x[Mg_{1/3}Nb_{2/3}]_{0.95}Ti_{0.05}B_yO_3$$

The doping content was $x = 0.01$ for A-site dopants and $y = 0.004$ for B-site dopants. Both dopants were introduced after the columbite phase formation, at the same time as lead oxide and titanium oxide, in the form described in Table 1.

Table 1. Dopants used

	Site A	*Site B*
Donor	La (La_2O_3)	W (WO_3)
Acceptor	Na (NaOH)	Al (Al_2O_3)
Mixed valency	Ag ($AgNO_3$)	Mn (Mn_3O_4)

The choice of dopants was conditioned by their ionic radius being small enough to allow them to enter the matrix. The sintering temperature was a function of the dopant in order to obtain samples with close microstructures and especially with equal grain size. The microstructure of all the samples was observed with an optical microscope and analysed using the software Visilog (Noesis). In this way a histogram of the grain size of the studied compositions is obtained. About one hundred grains were analysed in each case. The average grain size is between 3·4 and 4·9 μm. Non-doped La-, W-, Mn- and Na-doped samples were sintered at 950°C, while Ag- and Al-doped ones were sintered at 1100°C.

Powders were uniaxially pressed into discs. After the sintering process the samples are 0·5 mm thick and 7·5 mm in diameter. A 10-nm chromium underlayer is sputtered to ensure a good sticking of the electrodes on the ceramic then 0·5-μm gold electrodes are evaporated. By these means good and symmetrical electrical contacts can be achieved, allowing precise field determination.

3 Electrical Measurements

The accelerated degradation test was performed in a 300°C oven (Heraeus) with a 40-sample holder

installed on the back of the door. High-voltage coaxial connectors are disposed on the front of the door and permit an electrical link to resistors which sense the leakage current. These are scanned by a HP 3997A data acquisition unit. The electrical scheme of a single unit of measurement is shown in Fig. 1. The input resistor is for protecting the power supply in case of breakdown of a device under test (DUT); its value is chosen in order to allow the 90-V ignitor to trigger, lowering the voltage on the microvoltmeter of the HP 3997A and increasing the current through the 50-mA fuse which finally opens the circuit. The flashed DUT is then isolated from the others and the experiment can be performed until all the DUT are in short circuit. The HP controller monitors all the 40 insulation resistances by sampling them in a logarithmic timescale, in live or background mode. The $R(t)$ curve can be displayed for each sample without interruption of the scanning.

Several tests were made on samples of the same composition to check the reproducibility of the experiment. It was found that the degradation curves for the same composition are parallel, with only the initial values of the insulation resistance differing from one sample to another.

After the degradation test (lasting up to 11 days), the samples are cooled to room temperature with the voltage applied on them. Then they are disposed in a low-temperature oven in order to measure the ferroelectric hysteresis loop. The measurement is made with a modified Tower-Sayer circuit at 0·15 Hz. A triangular continuous wave is sent to a bipolar high-voltage power supply (Equipements Scientifiques) giving voltage between -1 and 1 kV. The charge amplifier is made with a high-input impedance operational amplifier in parallel with a 1-μF capacitor. The eventual offset due to the drift of the integration capacitance is numerically cancelled. The output is connected to a 12-bit digital scope (Nicolet 310) monitored by a MacIntosh II working under the Labview environment (National Instruments). The software makes the calculation of the positive and negative coercive fields E_c^+ and E_c^-, of the remanent polarization P_r^+ and P_r^- and of the saturation polarization P_s from the 4000 points of acquisition. The precision is better than 1 V for E_c and better than 1 μC/cm^2 for P. Thus very small shifts in the hysteresis loops can be seen as related to the material.

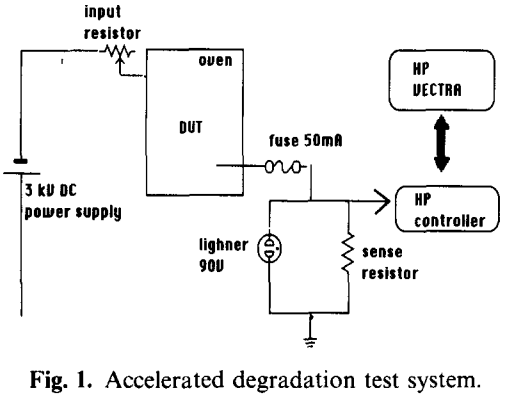

Fig. 1. Accelerated degradation test system.

4 Degradation Properties

Degradation of perovskite materials (ceramics and monocrystals) has been studied by Waser *et al.*,[5] who developed a model based on electromigration of oxygen vacancies under the DC field. The decrease in resistivity observed after a more or less long relaxation time is due to the formation of a *p–n* junction between two semiconductive regions. Whatever the initial conductivity type (*n* or *p*) of the material, this model can be used as the basis for oxide degradation provided that a high-temperature equilibrium between $V_O^{\cdot\cdot}$ and an acceptor defect has been established, with the acceptor defects frozen in the matrix and the donor not frozen.

The role of the grain boundaries has also been extensively modelled by this group, and pointed out in the case of PMN by Gaucher *et al.* in a recent paper.[6] However, for this study, the authors have focused on the intrinsic properties of the material by comparing ceramics with similar grain size distribution.

4.1 Donor-doped materials

A comparison of non-doped and La-doped materials in Fig. 2 shows that degradation is increased with the addition of the dopant. After 278 h the insulation resistance of the doped material is more than one decade lower than the maximum value. In contrast, the degradation of non-doped

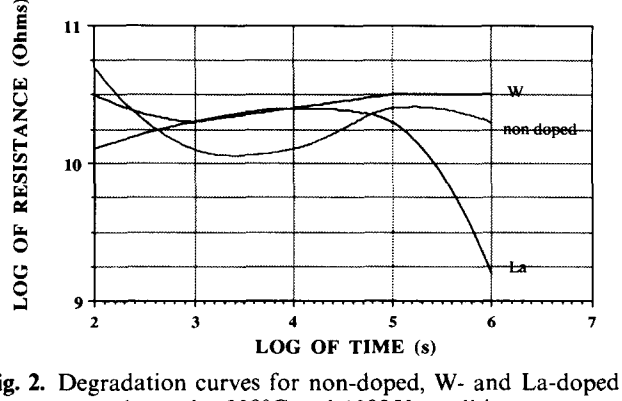

Fig. 2. Degradation curves for non-doped, W- and La-doped samples under 200°C and 1000 V conditions.

material decreased at the beginning of the test, but further degradation is very slow. This observation suggests that an increase of $V_O^{\cdot\cdot}$ defects has occurred, contrary to the usual effect of donor doping in perovskites.

Donor doping in site A with lanthanum has been extensively studied by Harmer and co-workers[2] and de Mathan.[3] The effect of this dopant is to enter preferentially into the ordered domains because of the lowering of their electrical charge. In theory the structure can become totally ordered according to the formula

$$Pb_{1-y}^{2+}La_y^{3+}(Mg_{(1+y)/3}Nb_{(2-y)/3})O_3$$

for $y = 0{\cdot}5$.[7]

For only 1% of La, only the size x of the ordered domains (see Introduction) is increased. This results in an effect opposite to that expected in the case of donor doping in a perovskite; if it is assumed that the ordered domains act as acceptor defects, they are likely to be compensated at high temperature by oxygen vacancies $V_O^{\cdot\cdot}$. The increase of their size would be related to an increase of the $V_O^{\cdot\cdot}$ concentration, contrary to the effect usually observed in barium or strontium titanate. The strong degradation observed on Fig. 2 for La-doped material compared with non-doped material is consistent with this model.

Donor doping in site B by tungsten ion shows an improvement in degradation properties (Fig. 2). In this case it can be assumed that the dopant goes into the disordered phase and acts as a conventional donor dopant. The decrease of $V_O^{\cdot\cdot}$ associated with the presence of tungsten ions would explain the lower degradation.

4.2 Acceptor-doped material

The effect of A-site (with Na) or B-site (with Al) substitution on degradation is shown in Fig. 3. Both dopants increase the degradation compared to non-doped material. A higher temperature than that used in the previous experiment has been shown because of the better reliability of these materials compared with those doped with La and W. (This fact explains why on Figs 2 and 3 the non-doped samples do not have the same behaviour, the temperature being different.) For Al-doped material the relaxation time is larger than for Na-doped material, but the following degradation is more abrupt.

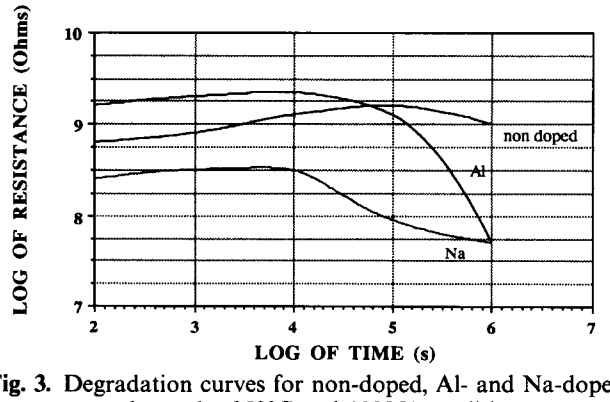

Fig. 3. Degradation curves for non-doped, Al- and Na-doped samples under 250°C and 1000 V conditions.

It should be expected that Na substitution on the A site has the opposite effect to La, that is a decrease of the ordered domain size, and consequently a decrease in $V_O^{\cdot\cdot}$. In fact, the decrease of domain size has been observed for Na doping content of 5 mol%.[2] In the present study the Na doping content is only 1 mol% and a reduction of the ordered domain size is not assumed. Another mechanism could explain the behaviour of the Na-doped sample. These dopants could act as conventional acceptor defects compensated at high temperature by oxygen vacancies. The increase in $V_O^{\cdot\cdot}$ should explain the increased degradation according to the classical model.

4.3 Mixed valency dopants

These dopants have been chosen because they can behave as acceptors (Ag^+ in an A^{2+} site or Mn^{2+} or Mn^{3+} in a B^{4+} site) at high temperature, fixing the $V_O^{\cdot\cdot}$ concentration, and achieve higher valency during cooling by an exothermic oxidation effect (Ag^{2+} and Mn^{3+} or Mn^{4+}).

Ag-doped samples have quite a similar degradation behaviour to non-doped samples (Fig. 3), except that they have more frequently abrupt breakdown due to process defects (this kind of random degradation is not investigated in this paper). The ceramic microstructure is not so regular and shows imperfections due to lower sintering capabilities. Despite this effect, some samples passed the whole degradation test and showed no difference to the non-doped samples.

The reoxidation property of the silver explains well this absence of difference: the high-temperature oxygen vacancies associated with acceptor Ag^+ ions are suppressed during cooling because of the reoxidation of Ag^+ to Ag^{2+}. The resulting material has only isovalent Ag^{2+} defects having no effect on degradation.

In contrast, Mn-doped samples have a very stable degradation curve (Fig. 4). This observation is surprising because this dopant is known as carrying reliability problems in barium titanate ceramics[8] (it is commonly used to allow sintering in an inert atmosphere with base metal electrodes). Once again, the PMN-based material has the opposite behaviour

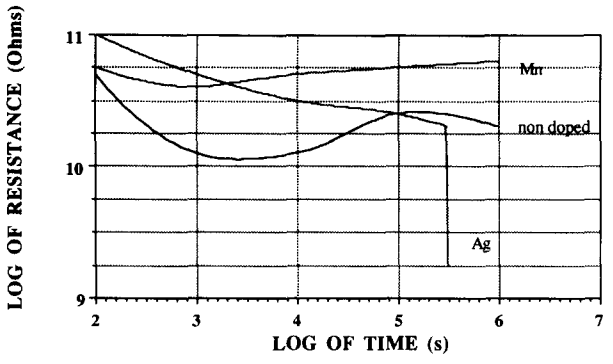

Fig. 4. Degradation curves for non-doped, Mn- and Ag-doped samples under 200°C and 1000 V conditions.

towards degradation compared with alkaline earth titanates, and even compared with a classical acceptor dopant in PMN. This effect can be explained by a study of the low-temperature ferroelectric properties.

5 Low-temperature Ferroelectric Properties

Hysteresis loops at −50°C for virgin and degraded samples were compared. Table 2 shows the results obtained for doped samples, non-doped sample being the reference material. Rectangularity is defined as the ratio P_r/P_s and internal field as $(E_c^+ + E_c^-)/2$. Of course, virgin samples have a null internal field.

For the non-doped material the saturation and remanent polarization values are lower after the degradation test (see also Fig. 5). A slight shift of the loop towards positive fields (direction of the applied DC field during the degradation test) reveals a small internal field of 10 V/mm for the degraded sample.

The La-doped material has a very slim loop (Fig. 6), as already shown in Ref. 3. This is due to the increase of the size of the ordered domains supposed

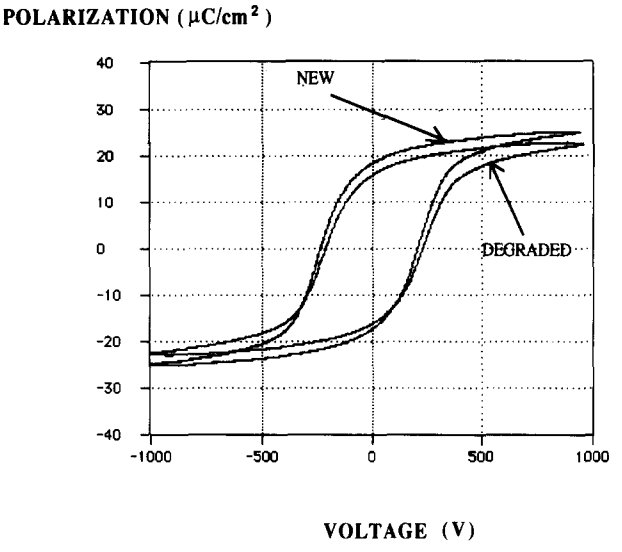

Fig. 5. Hysteresis loops for the non-doped sample before and after the degradation test.

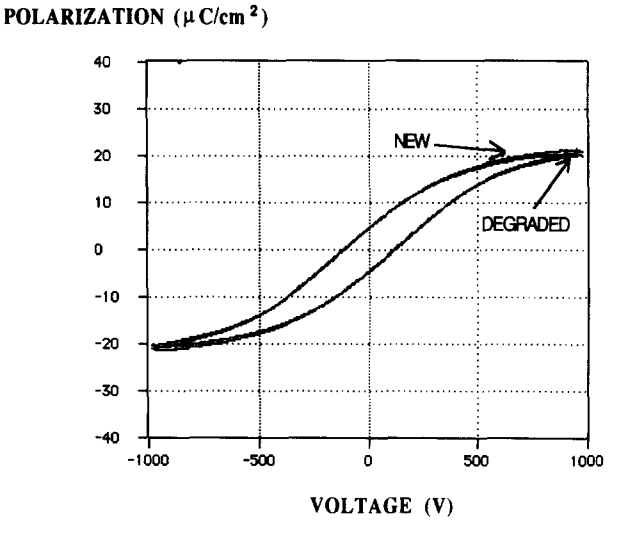

Fig. 6. Hysteresis loops for the La-doped sample before and after the degradation test.

Table 2. Ferroelectric measurements results

	Coercive field (V/mm)		*Rectangularity*		*Internal field (kV/m)*
	New	*Degraded*	*New*	*Degraded*	*(degraded)*
Non-doped	220	210	0·72	0·68	10
Donor doped					
La	130	130	0·18	0·11	0
W	240	250	0·74	0·74	20
Acceptor doped					
Na	200	195	0·63	0·6	0
Al	300	320	0·75	0·74	0
Mixed valency doped					
Ag	197		0·36		—
Mn	200	200	0·72	0·85	60

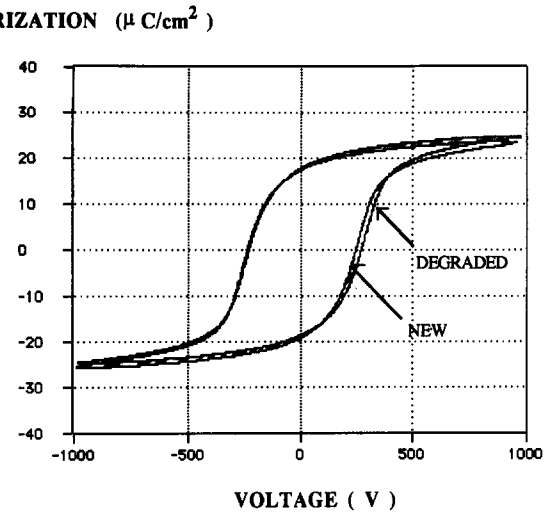

Fig. 7. Hysteresis loops for the W-doped sample before and after the degradation test.

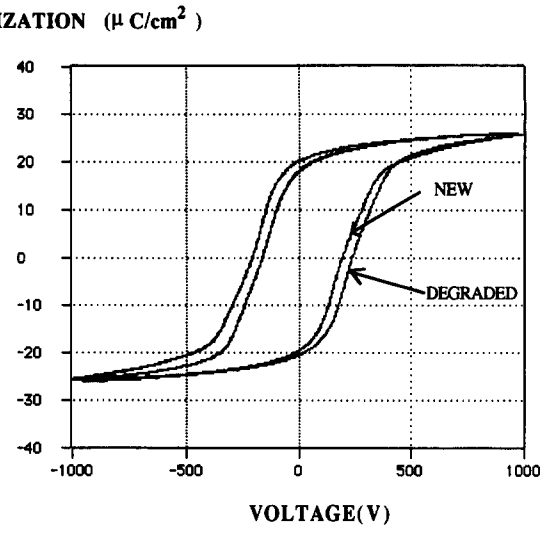

Fig. 9. Hysteresis loops for the Mn-doped sample before and after the degradation test.

to be responsible for the diffuse behaviour of the transition. The internal field after degradation is zero.

The W-doped material has a square loop with higher rectangularity than the non-doped one, but the main difference is the presence of an internal field (20 V/mm) after degradation and the absence of decrease of P_r and P_s (Fig. 7).

For the Na- and Al-doped materials no internal field was observed after degradation. Despite the very strong decrease of resistance during the accelerated life test, the loop is very similar before and after degradation (Fig. 8).

The Mn-doped material has a high rectangularity and a strong internal field after the degradation test (Fig. 9). This shift of the loop was stable after multiple cycling, but an ageing effect was observed when the sample was kept at room temperature during several days. The internal field tends to vanish, showing the reversible character of this effect.

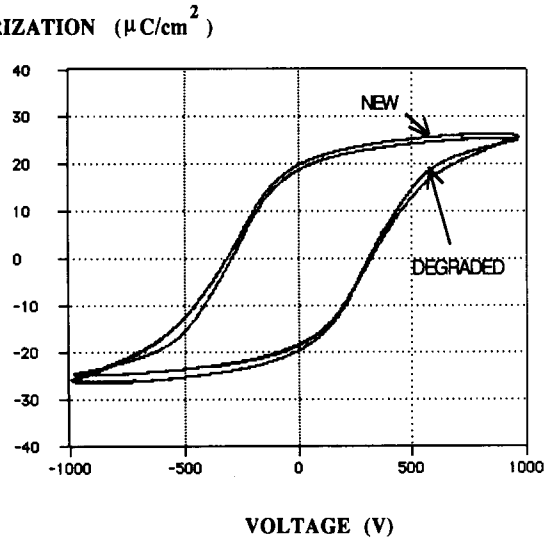

Fig. 8. Hysteresis loops for the Al-doped sample before and after the degradation test.

6 Discussion

It is surprising to note that the most degraded samples have the smallest change for the hysteresis loop after the degradation test. The samples doped with Mn and W, which have the best stability during the degradation test, have an internal field E_i when frozen down to the ferroelectric phase at −50°C. So the internal field is favourable to the life test endurance.

The work of Pan *et al.*[9] has shown that the Mn-doped PMN–PT materials have a larger ageing (in the absence of DC bias) than the non-doped ones. They explain this phenomenon by the presence of associated defects ($Mn''_B - V_O^{\cdot\cdot}$), which pin the ferroelectric domains and prevent them from switching under the AC field. The relaxation effect being shifted towards lower frequencies, the 1 kHz capacitance is lowered. Without any external bias field E_b, the dipoles ($Mn''_B - V_O^{\cdot\cdot}$)orient because of the depolarizing field of the ferroelectric domains that they tend to decrease. Their orientation is thus random.

During a degradation test the same dipoles are oriented by the DC field E_b in the paraelectric phase and keep their orientation during cooling down to the ferroelectric phase. They generate a non-isotropic internal field E_i that has been observed on the ferroelectric loops.

If this field can be measured only at low tempera-

ture by the use of ferroelectric measurements, it is likely to exist at higher temperature. The total field seen by the oxygen vacancies $V_O^{\cdot\cdot}$ is equal to

$$E_t = E_b - E_i$$

It is lower because of the presence of the associated defect. So the electromigration of the $V_O^{\cdot\cdot}$ is slower for Mn- and W-doped materials. This explains their improved degradation properties.

The internal field in W-doped samples can also be explained by the formation of associated defects $(V''_{Pb} - W^{\cdot\cdot}_B)$. W acts as a conventional donor impurity so as to decrease the $V_O^{\cdot\cdot}$ content and can even induce the formation of V''_{Pb} in order to compensate for the charge unbalance due to the +6 valency of the tungsten ion in the B sublattice.

7 Conclusion

A correlation has been observed between degradation of doped materials and internal field measured from the hysteresis loop at low temperature. The higher the lifetime, the higher the internal field. This has been interpreted by the presence of associated dipolar defects which minimize the total field inside the material. The migration of the oxygen vacancies is thus slowed down and the lifetime of the device is increased.

Acknowledgement

This work was supported under contract by the French DRET-DGA Administration.

References

1. Smyth, D. M., Harmer, M. P. & Peng, P., *J. Am. Ceram. Soc.*, **72**(12) (1989) 2276–8.
2. Chen, J., Chan, H. & Harmer, M. P., *J. Am. Ceram. Soc.*, **72**(4) (1989) 593–8.
3. de Mathan, N., PhD thesis, Ecole Centrale de Paris, 1991.
4. Shrout, T. R. & Halliyal, A., *Am. Ceram. Soc. Bull.*, **66**(4) (1987) 704–11.
5. Waser, R., Baiatu, T. & Härdtl, K. H., *J. Am. Ceram. Soc.*, **73**(6) (1990) 1663–73.
6. Gaucher, P., Noblanc, O., Deljurie, C. & Beauger, A., *European Ceramic Society Conference (ECERC'2)*, Augsburg, Germany, 11–14 September 1991.
7. Lin, L. J. & Wu, T. B., *J. Am. Ceram. Soc.*, **74**(6) (1991) 1360–3.
8. Rödel, J. & Tomandl, G., *J. Mat. Sci.*, **19** (1984) 3515–23.
9. Pan, W. Y., Jiang, Q. Y. & Cross, L. E., *Ferroelectrics*, **82** (1988) 111–17.